

Relativistic Self-similar Dynamic Collapses of Black Holes in General Polytropic Spherical Clouds

Biao Lian^{1, 2} and Yu-Qing Lou¹ \star

¹*Department of Physics and Tsinghua Centre for Astrophysics (THCA), Tsinghua University, Beijing 100084, China*

²*Department of Physics, McCullough Building, Stanford University, Stanford, California 94305-4045, USA*

Accepted 2013 November 21. Received 2013 November 21; in original form 2013 August 28

ABSTRACT

We study the hydrodynamic self-similar mass collapses of general polytropic (GP) spherical clouds to central Schwarzschild black holes and void evolution with or without shocks. In order to grossly capture characteristic effects of general relativity (GR) outside yet close to the event horizon of a Schwarzschild black hole and to avoid mathematical complexity, we adopt the approximation of the Paczynski-Wiita gravity to replace the simple Newtonian gravity in our model formulation. A new dimensionless parameter s appears with the physical meaning of the square of the ratio of the sound speed to the speed of light c . Various self-similar dynamic solutions are constructed for a polytropic index $\gamma > 4/3$. Two (for small enough $s < 1$) or no (for large enough $s < 1$) expansion-wave collapse solutions (EWCSs) with central event horizons exist when $\gamma > 4/3$, representing the collapse of static singular GP spheres towards the central singularity of spacetime. Such GP spherical dynamic mass collapse is shown to be highly efficient for the rapid formation of supermassive black holes (SMBHs; mass range of $\sim 10^6 - 10^{10} M_{\odot}$) in the early universe or even hypermassive black holes (HMBHs; mass range of $\sim 10^{10} - 10^{12} M_{\odot}$) if extremely massive mass reservoirs could be sustained for a sufficiently long time, which may evolve into hard X -ray/gamma ray sources or quasars according to their surroundings. Self-similar dynamic solutions of a GP gas are also proposed for the stellar mass black hole formation during the violent supernova explosion of a massive progenitor star, the timescale of which is estimated of $\sim 10^{-3}$ seconds. Rebound shocks travelling in supernovae are also discussed based on our self-similar shock expansion solutions.

Key words: accretion, accretion discs—black hole physics—early Universe—hydrodynamics—quasars: general—supernovae: general

1 INTRODUCTION

Mass accretions and collapses of black holes, especially supermassive black holes (SMBHs), are commonly thought to be related to galaxy formations and powerful quasars, and are still not well understood. To date, extensive observations have shown strong evidences that SMBHs of $10^6 \sim 10^{10} M_{\odot}$ reside in the corresponding galactic nuclei and manifest novel nucleus properties (e.g. Begelman et al. 1984; Rees 1984; Kormendy & Richstone 1995; Magorrian et al. 1998; Marconi & Hunt 2003; Wandel 1999, 2002; Ferrarese & Ford 2005; Graham & Driver 2007; Lou & Jiang 2008; Lou & Wu 2012; Shen et. al. 2009; McConnell et al. 2011; Shen et. al. 2011). In particular, McConnell et al. (2011) indicate that the two ten-billion-solar-mass black holes at the centers of two giant elliptical galaxies NGC 3842 and NGC 4889 (typi-

cal brightest cluster galaxies – BCGs) tend to be much more massive and deviate from the well-known $M_{\text{BH}} - \sigma$ relation significantly (e.g. Lou & Jiang 2008). It is widely believed that SMBHs in galactic nuclei are closely related to the formation and violently active phenomena (AGNs and quasars) of their host bulges. Recent observations of luminous quasars with red shifts as high as $z = 7$ (e.g. Mortlock et. al. 2011) indicate SMBHs with $\sim 10^8 M_{\odot}$ or higher must have occurred in one billion years or so after the Big Bang of the Universe. Another interesting recent development is the possible formation of intermediate mass black holes (IMBHs) at the centers of globular clusters and the tentative observational evidence for this plausible scenario (Lou & Wu 2012 and references therein). In the past several decades, many research works focusing on mass accretions towards black holes have been done, most of which were based on an accretion disk structure (e.g. Lynden-Bell 1969; Shakura & Sunyaev 1973; Novikov & Thorne 1973; Lynden-Bell & Pringle 1974;

\star louyq@mail.tsinghua.edu.cn

Paczynski & Wiita 1980; Rybicki & Lightman 1979; Sunyaev & Titarchuk 1980; Haardt & Maraschi 1991, 1993; Shapiro et al. 1976). We here explore an alternative yet complementary scenario. In the very early universe before stages of galaxy formation, the distribution of cosmic matters may be much denser and structure-less. Angular momentum may not be enough to induce disks in the formation of proto-galaxies. The black hole growth process around such early stage may not be able to rely on a surrounding well-established accretion disk. Loosely bound systems of sub-galactic arising from weakly interacting dark matter may have provided hosts for early SMBHs and quasars (e.g. Peebles 1982; Blumenthal et al. 1984). Inhomogeneity of the cosmological space time may also be present (e.g. Tolman 1934; Guth 1981; Mukhanova et al. 1992; Lyth & Riotto 1999), so that large-scale fluctuations and remaining acoustic waves from the Big Bang can in principle induce considerable local mass density fluctuations (e.g. Lukash 1980; Ford & Parker 1977), yielding high mass density peaks in the vast space. Dense grossly spherical blobs with or without central black holes born in such environments might experience quite novel dynamic mass collapse processes (Hoyle & Fowler 1963; Fowler 1964; Begelman 2009). In addition to disk-type accretion models, grossly spherical symmetric dynamic mass collapses may become another significant yet simplified model for most such early black hole evolution processes, which is the focus of this paper. In the literature, spherical accretion models like Bondi accretion are also used as simple estimation of mass accretion rates around compact objects (Bondi 1952; Bondi & Hoyle 1944; Mocanu 2012). We expect our dynamic spherical models would be useful for describing characteristics of mass inflows before the formation of a stable accretion disk structure inside the galactic nuclei.

There has been extensive investigations on the mass accretion and collapse of spherical gas clouds towards central massive objects through construction of spherical hydrodynamic self-similar solutions (e.g., Shu 1977; Whitworth & Summers 1985; Lou & Shen 2004; Lou & Cao 2008; Wang & Lou 2008). Most researchers so far work in the framework of Newtonian gravity which cannot give an exact description around highly general relativistic compact objects such as black holes to allow for a massive compact object occupying a very much smaller spatial volume, sitting at the center of $r = 0$. The physical behaviours of dynamic mass accretions and collapses close to a black hole then cannot be described more precisely. The construction of self-similar hydrodynamic gravitational collapse solutions using general relativity was done several years ago by Cai & Shu (2005), which describes a collapse of relativistic singular isothermal sphere (SIS) which is initially unstable (Cai & Shu 2003). Such solution construction involving general relativity is complicated and is done for isothermal sphere with a polytropic exponent $\gamma = 1$. In order to remedy the deficiency of Newtonian gravity while at the same time circumvent the mathematical machinery of general relativity and study the gravitational collapse of GP spheres, we invoke the Paczynski-Wiita potential (Paczynski & Wiita 1980) as a first-order correction of Newtonian gravity which is the weak field approximation of general relativity, and construct spherical self-similar gravitational collapse solutions of GP gas spheres. Under the approximation of the Paczynski-Wiita potential, the compact object has a finite Schwarzschild radius, and

many properties of spacetime near a black hole are reproduced approximately (Paczynski & Wiita 1980; Abramowicz 2009).

When relativistic conditions are introduced, solutions governed by the Paczynski-Wiita potential are significantly distinct from those in the framework of Newtonian gravity. Such conditions may occur in stellar core collapses and supernova explosion processes in accompany with the formation of a nascent neutron star or black hole (e.g. Chandrasekhar 1935; Oppenheimer & Volkoff 1939). Such highly relativistic dynamic processes will involve tempestuous changes in spacetime metric as well as gas inflows and need to be described by general relativity (Oppenheimer & Snyder 1939; Tolman 1939; Misner & Sharp 1964, 1965; Misner 1965). Realistic supernova processes also involve many other physics including radiation, heat transfer and production or annihilation of leptons and neutrinos (e.g. Bethe 1990), and thus remains still a major unsolved astrophysical problem. Despite of much complexities in supernova physics, we wish to focus on the hydrodynamic part, give several estimates, and catch some basic features of the supernova such as the timescale of the formation of a stellar black hole.

The remainder of the paper is structured as follows. In Section 2, the basic nonlinear hydrodynamic partial differential equations (PDEs) and the corresponding reduced ordinary differential equations (ODEs) for constructing the important class of self-similar hydrodynamic solutions are introduced and derived. In Section 3, we consider several asymptotic analytic solutions of the coupled nonlinear ODEs, indicating key differences of solutions in our model formalism as compared to those obtained by others previously using the Newtonian gravity. Explicit numerical solutions of various kinds including shock waves and/or central voids are shown and analyzed in Section 4. Section 5 describes the physical consequences closely related to self-similar hydrodynamic solutions obtained in this paper, and conclusions are summarized in Section 6. Three appendices of more detailed mathematical analysis are attached for the convenience of references.

2 THE BASIC MODEL DESCRIPTION

In our model formalism, the gravity force under the approximation of the Paczynski-Wiita potential is adopted instead of the Newtonian gravity force to include certain effects of general relativity in a simplified manner. In our formalism, the Paczynski-Wiita gravity force per unit mass is

$$g = -\frac{GM}{(r - 2GM/c^2)^2}, \quad (1)$$

where $G = 6.67 \times 10^{-8} \text{g}^{-1} \text{cm}^3 \text{s}^{-2}$ is the universal gravitational constant, r is the radius from the center, $c = 3 \times 10^{10} \text{cm s}^{-1}$ is the speed of light and M is the total mass enclosed inside a mass sphere of radius r . In reference to the Newtonian gravity, the extra term $2GM/c^2$ included here is the Schwarzschild radius for a non-rotating Schwarzschild black hole of an enclosed mass M . We emphasize that the specific gravity force g here is simply the gradient of potential $\phi = -GM/(r - 2GM/c^2)$ of Paczynski & Wiita (1980) for a constant enclosed mass M . As this expression of Paczynski-Wiita potential ϕ is not consistent

with the self-gravity as stipulated by the Poisson equation relating the gravitational potential ϕ and the mass density ρ , we no longer require the Poisson equation which ensures that the gravity force is produced solely by the enclosed mass M . To justify our approximation, we demand the mass density being sufficiently low (at most proportional to r^{-2} , see subsection 3.2) in the asymptotic regime of $r \rightarrow +\infty$.

We emphasize that the Paczynski-Wiita potential captures well the deviation from the r^{-1} law of the Newtonian gravitational potential for an extremely dense object (e.g. Abramowicz 2009) – an essential element of our paper, and thus can reproduce the characteristic features of general relativity. Combined with non-relativistic particle kinetics in circular Keplerian orbits, it gives exactly the same radii of the marginally stable orbit (r_{ms}) and the marginally bound orbit (r_{mb}) as those given by Einstein’s general relativity (Paczynski & Wiita 1980), which justifies the validity of this “pseudo Newtonian” approximation. For the historical background, theoretical development and a step-by-step “derivation” of the Paczyński-Wiita potential as well as comparisons with Einstein’s general relativity, the interested reader is referred to the two-page commentary of Abramowicz (2009) for more details. There are other proposed potentials (e.g., Nowak & Wagoner 1991; Semerák & Karas 1999; Kluźniak & Lee 2002; Stuchlík & Kovár 2008) with respective merits to capture features of general relativity, we adopt the Paczyński-Wiita potential here mainly for beauty and simplicity.

In a reference framework of spherical polar coordinates (r, θ, ϕ) , the basic nonlinear hydrodynamic PDEs for a spherically symmetric dynamic evolution of a GP gas are given below in the forms of

$$\frac{\partial \rho}{\partial t} + \frac{1}{r^2} \frac{\partial}{\partial r} (r^2 \rho u) = 0, \quad (2)$$

$$\frac{\partial M}{\partial t} + u \frac{\partial M}{\partial r} = 0, \quad (3)$$

$$\frac{\partial M}{\partial r} = 4\pi r^2 \rho, \quad (4)$$

$$\frac{\partial u}{\partial t} + u \frac{\partial u}{\partial r} = -\frac{1}{\rho} \frac{\partial p}{\partial r} + g, \quad (5)$$

where t is the independent time variable, ρ , p and u are the gas mass density, the gas pressure and the radial flow velocity of the gas, respectively, and the gravity force per unit mass g is given by equation (1) in the Paczynski-Wiita approximation. By further demanding the conservation of specific entropy along streamlines, we have

$$\left(\frac{\partial}{\partial t} + u \frac{\partial}{\partial r} \right) \ln \left(\frac{p}{\rho^\gamma} \right) = 0, \quad (6)$$

where γ is the polytropic index of a dynamic gas. PDEs (3) and (6) bear the same form which implies the involvement of enclosed mass in the GP EoS as discussed presently.

We now introduce in a self-consistent manner the following self-similarity transformation,

$$\begin{aligned} r &= k^{1/2} t x, & u &= k^{1/2} v(x), & \rho &= \frac{\alpha(x)}{4\pi G t^2}, \\ p &= \frac{k \beta(x)}{4\pi G t^2}, & M &= \frac{k^{3/2} t m(x)}{G}, \end{aligned} \quad (7)$$

such that nonlinear hydrodynamic PDEs (1)–(5) can be consistently and readily reduced to a set of coupled nonlinear ODEs in terms of the independent self-similar variable x . Here, dimensionless dependent variables $v(x)$, $\alpha(x)$, $\beta(x)$, $m(x)$ are four reduced functions of x only. The sound parameter k is an allowed scaling factor to solve the coupled nonlinear ODEs. The self-similar scaling index n is simply set to unity from the very beginning for a successful transformation (e.g. Wang & Lou 2008; Lou & Shi 2013). For the mass conservation, nonlinear PDEs (3) and (4) together lead to

$$m = (x - v)x^2 \alpha, \quad (8)$$

and in order that the enclosed mass M remains positive, the inequality $x - v > 0$ must be met as dictated by physics. For the point keeping $x - v = 0$, the enclosed mass is zero and we would have an expanding central void. The form of reduced pressure $\beta(x)$ is determined by PDE (6) to be

$$\beta = \mathcal{C} \alpha^\gamma m^{2(\gamma-1)}, \quad (9)$$

where \mathcal{C} is a constant proportional coefficient. Here, we shall not consider the special case of $\gamma = 4/3$ for a relativistically hot or degenerate gas (e.g., Lou & Cao 2008); by properly adjusting the scaling factor k , we can always make the coefficient $\mathcal{C} = 1$ without loss of generality, leading to the following simple algebraic form of $\beta(x)$

$$\beta = \alpha^\gamma m^{2\gamma-2} = \alpha^{3\gamma-2} (x - v)^{2\gamma-2} x^{4\gamma-4} \quad (10)$$

in reference to two algebraic relations (8) and (9). The remaining two nonlinear PDEs (2) and (5) give the following two coupled nonlinear ODEs

$$(x - v) \left(\frac{2\alpha}{x} + \frac{d\alpha}{dx} \right) = \alpha \frac{dv}{dx}, \quad (11)$$

$$\frac{1}{\alpha} \frac{d\beta}{dx} - (x - v) \frac{dv}{dx} = -\frac{(x - v)x^2 \alpha}{[x - s(x - v)x^2 \alpha]^2}, \quad (12)$$

where reduced pressure $\beta(x)$ is given by algebraic equation (10), and $s = 2k/c^2$ is a constant parameter proportional to the square of the ratio of sound speed over the speed of light c . Nonlinear ODEs (11) and (12) can be readily rearranged into the following form of

$$\begin{aligned} \left[(x - v)^2 - \gamma \frac{\beta}{\alpha} \right] \frac{1}{\alpha} \frac{d\alpha}{dx} &= \frac{(x - v)x^2 \alpha}{[x - s(x - v)x^2 \alpha]^2} \\ &+ \frac{2\gamma - 2}{(x - v)} \frac{\beta}{\alpha} - \frac{2(x - v)^2}{x}, \end{aligned} \quad (13)$$

$$\begin{aligned} \left[(x - v)^2 - \gamma \frac{\beta}{\alpha} \right] \frac{1}{(x - v)} \frac{dv}{dx} &= \frac{(x - v)x^2 \alpha}{[x - s(x - v)x^2 \alpha]^2} \\ &+ \left(\frac{2\gamma - 2}{x - v} - \frac{2\gamma}{x} \right) \frac{\beta}{\alpha}. \end{aligned} \quad (14)$$

Nonlinear ODEs (13) and (14) can be readily solved by standard numerical integration with specified asymptotic conditions and/or solutions which we elaborate next.

3 ASYMPTOTIC ANALYTIC SOLUTIONS

By some sensible physical assumptions and requirements, asymptotic analytical solutions within certain parameter regimes can be derived. These asymptotic behaviors are very

valuable and useful for constructing and understanding the numerical solutions.

3.1 Asymptotic analytic solutions of finite mass density and velocity at large x

For asymptotic analytic solutions with $\alpha(x)$ and $v(x)$ approaching finite values at very large x , nonlinear ODE (11) in the leading order can be approximated as

$$\frac{2\alpha}{x} + \frac{d\alpha}{dx} = 0, \quad (15)$$

yielding the asymptotic solution for $\alpha(x)$ at $x \rightarrow +\infty$

$$\alpha = \frac{\alpha_0}{x^2} + o\left(\frac{1}{x^2}\right). \quad (16)$$

Asymptotic solution (16) further leads to the leading order approximation of ODE (14) at very large x as

$$\frac{dv}{dx} = -\left[2\alpha_0^{3\gamma-3} - \frac{\alpha_0}{(1-s\alpha_0)^2}\right] \frac{1}{x^2}, \quad (17)$$

and the corresponding asymptotic solution of $v(x)$ at very large x is therefore

$$v(x) = v_0 + \left[2\alpha_0^{3\gamma-3} - \frac{\alpha_0}{(1-s\alpha_0)^2}\right] \frac{1}{x} + o\left(\frac{1}{x}\right). \quad (18)$$

For a realistic astrophysical consideration, we shall demand $s\alpha_0 < 1$ for the space-time domain outside the event horizon of a central Schwarzschild black hole. This constraint is in fact due to the invalidation of the Paczynski-Wiita potential at high mass densities of infinite radius (the Poisson equation is no longer imposed here, see Section 2). In most realistic astrophysical flow systems, indeed, the gas density far away enough will always decrease sufficiently fast and go below this critical value of unity for $s\alpha_0$. Asymptotic solution (18) can be used to further obtain the expression of $\alpha(x)$ to the second order in the form of

$$\alpha = \frac{\alpha_0}{x^2} \left\{ 1 + \left[2\alpha_0^{3\gamma-3} - \frac{\alpha_0}{(1-s\alpha_0)^2}\right] \frac{1}{2x^2} \right\} + o\left(\frac{1}{x^4}\right). \quad (19)$$

By setting $s = 0$ in the above two expressions, we readily recover the Newtonian results, and the above asymptotic analytical solutions carry the same form as those deduced in previous works with $n = 1$ for the Newtonian gravity (e.g. Wang & Lou 2008; Lou & Shi 2013) as expected. Clearly, $s \neq 0$ is the key difference brought by the Paczynski-Wiita gravity. It greatly enriches the possible classes of self-similar dynamic solutions with event horizons and central expanding voids, as revealed by numerical solutions in Section 4.

We shall presently discuss direct applications of these asymptotic analytical solutions at large enough x for numerical integrations of coupled nonlinear ODEs (13) and (14) using the standard Runge-Kutta shooting scheme.

3.2 The absence of asymptotic analytic solutions for thermal expansion at large x

Wang & Lou (2008) derived asymptotic self-similar solution for magnetohydrodynamic (MHD) thermal expansion at large x (also Wang & Lou 2007). In this subsection, we naturally examine this possibility by removing the magnetic field and by invoking the Paczynski-Wiita gravity in the

form of expression (1). For such a thermal expansion, we expect $v(x)$ to be proportional to x as $x \rightarrow \infty$, namely

$$v(x) = bx + o(x), \quad (20)$$

where b is a constant proportional coefficient. Then nonlinear ODE (11) can be approximately written as

$$\frac{d\alpha}{dx} + \frac{(2-3b)\alpha}{(1-b)x} = 0, \quad (21)$$

giving the leading order term of $\alpha(x)$ as

$$\alpha = \alpha_e x^{-(2-3b)/(1-b)} + \dots, \quad (22)$$

where α_e is a constant proportional coefficient. In order that the factor in the denominator $[x - s(x-v)x^2\alpha]$ of our nonlinear ODEs to be positive definite at large x , the leading order term of α when $x \rightarrow \infty$ can at most be of power -2 for x . This is also the condition for our approximate gravity force (1) to be valid. With this consideration, we require

$$(2-3b)/(1-b) \geq 2. \quad (23)$$

Here we take b parameter to be non-zero and thus the above inequality demands $b \leq 0$, which would correspond to a homogeneous asymptotic collapse instead of an expansion. However, the leading order of ODE (14) then gives

$$(1-b)b = 0, \quad (24)$$

indicating no such solutions can exist. The absence of thermal expansion or collapse solutions here is also due to the invalidity of the approximate gravity force under such conditions, since the outside gas mass density is not low enough.

3.3 Asymptotic analytic solutions of a diverging radial flow velocity $v(x)$ at a finite x

We here consider that $v(x)$ diverges at a finite value $x = x_1$; this point expands with time in a self-similar manner. Then in the vicinity of x_1 , $v(x)$ becomes the dominant term, and nonlinear ODE (11) bears the local asymptotic form of

$$\frac{d(x^2\alpha)}{x^2\alpha} + \frac{dv}{v} = 0, \quad (25)$$

immediately leading to

$$-x^2\alpha v \rightarrow m_0, \quad (26)$$

where m_0 is a positive constant of integration with the physical meaning of the enclosed mass within $x = x_1$ or the mass accretion rate there. We presume that the divergent $v(x)$ behavior results from the approaching zero behavior of the denominator $[x - s(x-v)x^2\alpha]$ in our nonlinear ODEs, which has the asymptotic form according to the above discussion (as will be shown later α approaching zero there)

$$x - s(x-v)x^2\alpha \rightarrow x - sm_0. \quad (27)$$

We therefore identify the divergent point as $x_1 = sm_0$. Physically, we have $s > 0$. Together with the condition of $\gamma \geq 1$ (which is almost always true), we verify that the ratio $\beta(x)/\alpha(x)$ remains finite at $x = sm_0$. Consequently, the asymptotic form of nonlinear ODE (14) becomes

$$-v \frac{dv}{dx} = \frac{m_0}{(x - sm_0)^2}. \quad (28)$$

The corresponding asymptotic solution $v(x)$ diverges near $x_1 = sm_0$ in the leading-order form of

$$v = -\left(\frac{2m_0}{x - sm_0} + v_d^2\right)^{1/2}, \quad (29)$$

where $v_d > 0$ is a positive constant of integration. Here, $x_1 = sm_0$ would correspond to the expanding boundary (event horizon) of a Schwarzschild black hole harbored at the center. This implies in turn that the reduced mass density $\alpha(x)$ approaches zero fast enough in the vicinity of a Schwarzschild black hole boundary, namely

$$\alpha = \left[s^2 m_0 \left(\frac{2m_0}{x - sm_0} + v_d^2\right)^{1/2}\right]^{-1}. \quad (30)$$

Accordingly and as a result of sustained dynamic mass collapse, the dimensional radius r_g of the Schwarzschild black hole with a mass M grows linearly with time t as

$$r_g = \frac{2GM}{c^2} = 2ct \left(\frac{s}{2}\right)^{3/2} m_0. \quad (31)$$

In other words, the increasing rate of the Schwarzschild black hole radius is also directly related to m_0 parameter.

In general relativity, the physical velocity is less than the speed of light c . To incorporate this effect into the Paczynski-Wiita gravity, one should actually relate the true physical velocity u_{tru} with the calculated velocity u by $u = u_{tru}/(1 - u_{tru}^2/c^2)$ (Abramowicz et. al. 1996; Abramowicz 2009). In this perspective, we interpret the divergence of u near the black hole event horizon as the true velocity u_{tru} approaches c .

3.4 Asymptotic analytic solutions for the radial flow velocity approaching zero at small x

First, we study the case when $v(x)$ becomes negligible as compared with x in the limit of $x \rightarrow 0$. Among others, we presume $v(x)$ in the power-law form of

$$v \rightarrow \Re\left(v_s x^P\right), \quad (32)$$

where v_s is a complex constant proportional coefficient in general and $\Re(\dots)$ operation takes the real part of the argument; while P is a complex index with its real part $\Re(P) > 1$. Conceptually, the imaginary part of P would lead to an oscillatory behavior of $v(x)$. Nonlinear ODE (11) then gives

$$\frac{1}{x^2 \alpha} \frac{d(x^2 \alpha)}{dx} = \Re\left(v_s P x^{P-2}\right), \quad (33)$$

which readily leads to an asymptotic solution of

$$\alpha \approx \frac{\alpha_s}{x^2} \left[1 + \Re\left(\frac{v_s P}{P-1} x^{P-1}\right)\right], \quad (34)$$

where α_s is a positive constant proportional coefficient resulting from the analytic integration. In this case, the mass $m(x)$ enclosed inside radius x carries the asymptotic behavior of $m \rightarrow \alpha_s x$. To ensure that the radius x remains always larger than the dimensionless Schwarzschild radius sm where our theoretical model applies, we would require $s\alpha_s < 1$. Substituting this approximate solution into nonlinear ODE (14) and keeping up to the second-order terms, we derive the following relation

$$\begin{aligned} & \frac{\alpha_s}{(1 - s\alpha_s)^2} \left\{1 + \Re\left[\left(\frac{1 + s\alpha_s}{1 - s\alpha_s} \frac{1}{P-1} - (3 - 2\gamma)\right) v_s x^{P-1}\right]\right\} \\ & = 2\alpha_s^{3\gamma-3} \left\{1 + \Re\left[\left(\frac{3\gamma-3}{P-1} - \gamma - \frac{\gamma P}{2}\right) v_s x^{P-1}\right]\right\}. \end{aligned} \quad (35)$$

Terms of the same powers of x on both sides of relation (35) should be equal; we then have separately the following algebraic equations for determining α_s

$$2\alpha_s^{3\gamma-4} (1 - s\alpha_s)^2 = 1, \quad (36)$$

and for determining the complex power index P

$$\gamma(P-1)^2 + (7\gamma-6)(P-1) + \frac{2(1+s\alpha_s)}{(1-s\alpha_s)} + 6 - 6\gamma = 0. \quad (37)$$

Practically, we may regard $(P-1)$ as an unknown variable to be determined. This is then a quadratic equation for variable $(P-1)$. We consider $\gamma \geq 1$, so $7\gamma-6 > 0$. According to our presumption, we want to find a root with $\Re(P-1) > 0$. Such a root of P is then impossible unless the constant term $2(1+s\alpha_s)/(1-s\alpha_s) + 6 - 6\gamma < 0$, namely

$$\gamma > 1 + \frac{(1+s\alpha_s)}{3(1-s\alpha_s)}. \quad (38)$$

In the Newtonian gravity limit of $s\alpha_s \rightarrow 0$, this inequality is just $\gamma > 4/3$. This condition also indicates P must be real, and so no oscillatory behavior would occur.

Another possible self-similar solution is that $v(x)$ is proportional to x near the center, namely $v \rightarrow v_s x$ with the proportional coefficient v_s satisfying $0 < v_s < 1$. To the leading order, nonlinear ODE (11) then gives

$$\alpha = \alpha_s x^{-2+v_s/(1-v_s)}. \quad (39)$$

This indicates the reduced enclosed mass $m = (1 - v_s)\alpha_s x^{v_s/(1-v_s)+1}$, dropping faster than x as $x \rightarrow 0$, so the dimensionless Schwarzschild radius sm remains smaller than x . Nonlinear ODE (14) would be different for different regimes of $\gamma \neq 4/3$ values. In the regime of $\gamma > 4/3$, it gives

$$\frac{v_s}{(1-v_s)} = 2, \quad v_s = 2/3, \quad (40)$$

and

$$\alpha_s = v_s = 2/3. \quad (41)$$

On the other hand for $\gamma < 4/3$, the second term on the right-hand side takes charge, and yields

$$-\gamma v_s = 2\gamma v_s - 2, \quad v_s = 2/(3\gamma), \quad (42)$$

where α_s can take on any positive value. For these asymptotic behaviors discussed here, there will be no Schwarzschild black holes at the center. For $\gamma > 4/3$, the reduced mass density $\alpha(x)$ approaches a constant α_s at $x = 0$, while for $\gamma < 4/3$, $\alpha(x)$ diverges as $x \rightarrow 0$.

4 CONSTRUCTION OF NUMERICAL SELF-SIMILAR DYNAMIC SOLUTIONS

By properly specifying various analytic asymptotic solutions, we could construct numerical solutions from two coupled nonlinear ODEs (13) and (14) by straightforward numerical integrations. We implement the fourth-order Runge-Kutta shooting scheme to integrate nonlinear ODEs (13) and (14) numerically with proper initial conditions. Then we

plot the negative radial flow speed $-v(x)$ versus the independent self-similar variable x . The critical curves of these two coupled nonlinear ODEs are found not to extend to infinity, instead they form closed loops when approaching large values of x , and sometimes they may even disappear, as shown below. This is an interesting novel feature of introducing the Paczynski-Wiita gravity in our self-similar hydrodynamic analysis. The behaviors of the solutions in the vicinity of critical curves are detailed in Appendix A.

4.1 Critical curves of the nonlinear ODEs and expansion-wave collapse solutions (EWCSs)

When the coefficients of dv/dx and $d\alpha/dx$ on the left-hand side (LHS) of nonlinear ODEs (13) and (14) become zero, the right-hand side (RHS) must vanish simultaneously in order to ensure finite values of first derivatives dv/dx and $d\alpha/dx$. These two conditions give the equation for the sonic critical curve of the two coupled nonlinear ODEs, viz.

$$\frac{(x-v)}{x} - \frac{\gamma-1}{\gamma} = \frac{\gamma^{\frac{1}{3-3\gamma}}(x-v)^{\frac{\gamma+1}{3\gamma-3}} x^{2/3}/2}{[x - s\gamma^{\frac{1}{3-3\gamma}}(x-v)^{\frac{\gamma+1}{3\gamma-3}} x^{2/3}]^2} \quad (43)$$

(see Appendix B for detailed derivations). For a necessary consistency, this result has been carefully checked against the pertinent results of Wang & Lou (2008). Sonic critical lines carry the physical meaning that they separate between supersonic and subsonic flows. It is obvious that for $\gamma > 1$, $x-v=0$ is a branch of the critical line. This line is special in the sense that it cannot be crossed, since we must require a positive enclosed mass $m = x^2\alpha(x-v)$ everywhere. Therefore, this straight line is referred to as the zero-mass line (ZML) for which the enclosed mass remains zero. For self-similar dynamic solutions touching the ZML, expanding voids emerge around the center and evolve with time t in a self-similar manner. Physically, a central energy supply (e.g. photon gas, high-energy neutrinos and/or electron-positron e^\mp pair plasma) would be required to initiate and sustain such void formation and evolution (e.g. Lou & Wang 2011).

The behavior of the second branch of the critical lines is found closely related to the number of roots of α_0 from the following equation

$$2\alpha_0^{3\gamma-4}(1-s\alpha_0)^2 = 1. \quad (44)$$

(see equations 17 and 18). The number of roots of equation (44) for various pair values of s and γ is shown in Figure 1 (see Appendix B for a detailed analysis). In the regime of $\gamma < 4/3$, there is always one root only for α_0 , and we refer to this regime as Type A. In the regime of $\gamma > 4/3$, there exists a curved boundary separating the ‘‘two roots’’ regime (referred to as Type B) and the ‘‘no root’’ regime (referred to as Type C). Note that for $s < (1 - \sqrt{2}/2) = 0.2929$ and $\gamma > 4/3$, there are always two roots for α_0 .

The sonic critical curve in general appears like a closed loop. In Figure 2, we show several such sonic critical curves for $s = 0.2929$ with different γ values ranging from 1.05 to 1.8; the straight ZML $x-v=0$ is not shown in this figure. In the Type A regime of $\gamma < 4/3$, the sonic critical loop curve touches the origin for the cases of $\gamma = 1.05, 1.2, 1.3$, respectively, and it seems that the loop ‘‘breaks’’ into two branches in the vicinity of the origin (e.g., see the sonic

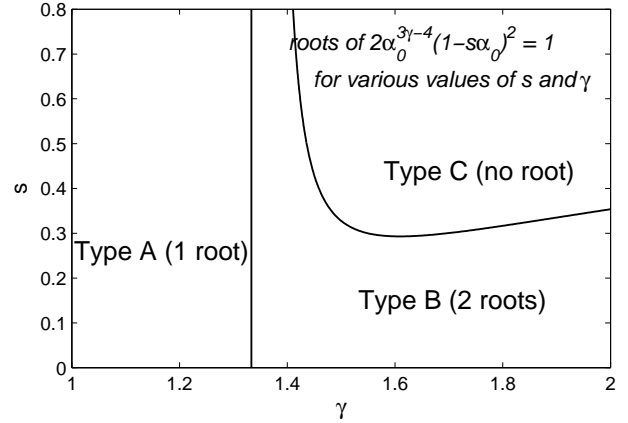


Figure 1. Different regimes for parameter pair s and γ , classified according to the number of α_0 roots of equation $2\alpha_0^{3\gamma-4}(1-s\alpha_0)^2 = 1$ (see Appendix B). The solid vertical line marks $\gamma = 4/3$. To the left of this $\gamma = 4/3$ vertical line (i.e., type A regime), there exists one root for α_0 . To the right of this $\gamma = 4/3$ vertical line, the solid curve separates the no root regime (i.e., type C) from the two root regime (i.e., type B) as indicated. Right along the $\gamma = 4/3$ vertical line, we would have two roots of $\alpha_0 = (1 \pm 1/\sqrt{2})/s$ (the plus sign root is unphysical), although the case of $\gamma = 4/3$ is not considered in this paper (see Goldreich & Weber 1980 and Lou & Cao 2008 for $\gamma = 4/3$ with the Newtonian gravity). Each root α_0 may correspond to an expansion-wave collapse solution (EWCS) with $\alpha = \alpha_0/x^2$ and $v = 0$ in the regime of very large x . In the type C regime, no sonic critical lines exist.

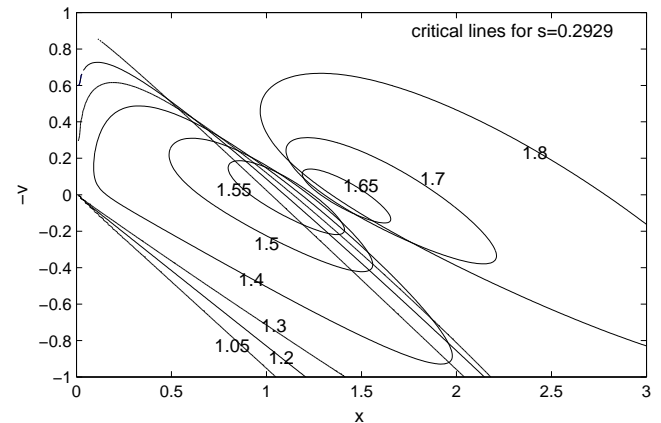


Figure 2. Sonic critical curves for different γ values marked along the curves all with the same value for $s = 0.2929$. For $\gamma < 4/3$, the critical curves touch the origin $x = 0, v = 0$; three examples are shown for $\gamma = 1.05, 1.2, 1.3$, respectively. For $\gamma > 4/3$ ranging from 1.4 to 1.8, the sonic critical lines form loops which shrink when the parameters approach the type C regime shown in Figure 1 (around $\gamma \sim 1.6$).

critical curve of $\gamma = 1.2$ in Figure 2 and also see the dash-dotted curve in Figure 6). It can be shown that the sonic critical curve touches the origin in the manner $v = x/\gamma$ (this would differ from the ZML for $\gamma > 1$ with different slopes). In the Type B regime, the critical curve forms a closed loop, and is away from the origin, as shown in Figure 2 (see also the dash-dotted curves in Figures 4 and 5). In the Type C regime, it is found that the sonic critical curve disappears

completely. In Figure 2, we observe how the closed sonic critical loop moves step by step when the parameter pair (γ, s) gradually approaches the Type C regime.

This behavior of the sonic critical curve becomes better understood as we explore numerically *expansion-wave collapse solutions* (EWCS), as first studied by Shu (1977) for an isothermal gas under the Newtonian self-gravity (see also further extensions by Lou & Shen 2004 and references therein). An EWCS contains an expansion wave front outside of which the gas remains static (in an equilibrium between the gas pressure and the self-gravity) and inside of which the gas gradually collapses towards a central free-fall to form a mass-accreting core, which would be a black hole with an event horizon in the present context. Basically, it describes a spontaneous collapse of a general static singular polytropic sphere (SPS) solution starting with a power-law mass density profile and zero velocity, i.e.

$$v(x) = 0, \quad \alpha(x) = \frac{\alpha_0}{x^2}, \quad (45)$$

where α_0 is the root of equation (44). A singular static gas sphere (be it isothermal, conventional polytropic or GP) results from the balance of pressure force and self-gravity and is generally considered as unstable in both the non-relativistic limit (e.g., Shu 1977; Lou & Shen 2004) and the relativistically hot or degenerate gas with $\gamma = 4/3$ (e.g., Cai & Shu 2003). Once an infinitely small expansion-wave front emerges from the central core region, the affected sphere will continuously collapse in a self-similar dynamic manner. The expansion wave front always lies on the sonic critical curve (see figure 2 of Shu 1977 for an isothermal gas; see also Tsai & Hsu 1995). It is then apparent that in the Type C regime where no α_0 root of equation (44) exists, there should be no EWCSs accordingly. In other words, there is no sonic critical curve available for the expansion wave front to sit at. Now we turn to Type B regime, where the sonic critical curve forms a closed loop away from the origin in a $-v$ versus x figure presentation. There are two roots of α_0 available for constructing the outside SPS solutions, and a numerical integration does give two possible EWCSs with two different event horizons. The two corresponding Schwarzschild radii increase with constant yet different speeds for the same s but different m_0 values. This is a novel feature of forming black holes in a static mass reservoir stretched to larger radii. In both Figures 4 and 5, the two EWCSs in each case are displayed by heavy solid curves. As is easily seen, different choices of α_0 give distinct locations of the expansion wave front. The loop shaped sonic critical curve cuts the horizontal x axis twice, and is exactly able to hold two expansion wave fronts, corresponding to the two roots of α_0 respectively. The outer (or faster) EWCS seems to be more “dense” than the inner one, in the sense that it corresponds to a higher α_0 value. In Type A regime, however, there is only one root of α_0 , and we thus expect only one EWCS, which is numerically verified indeed. In Figure 6 for $\gamma = 1.2$, such a solution is shown in heavy solid curve. It is also easy to understand this result from the perspective of the sonic critical curve. In this situation the sonic critical loop breaks, and is connected to the origin. So it cuts the positive x axis only once, and can only hold one expansion wave front. Based on the discussion above, we see that there exists a one-to-one correspondence between the behavior of

the sonic critical curve and the emergence of EWCSs with corresponding event horizons.

We note in particular that EWCSs shown above are quite different when the Paczynski-Wiita gravity is considered for the dynamic collapse of a GP gas sphere. We expect these EWCSs to be generally valid in the exact general relativity formalism, since the Paczynski-Wiita gravity closely approximates Einstein’s general relativity in describing the strong-field deviation of the gravitational potential from the $1/r$ law. Particularly, the discussion of EWCSs based on the number of roots of equation (45) is sufficiently general, and should depend little on the details of gravitational potential. Cai & Shu (2005) considered gravitational collapses in the general relativistic formalism for singular isothermal spheres (SIS) with $\gamma = 1$, and found only one EWCS. Our conclusions here are consistent with their results. More importantly, we emphasize that for $\gamma > 4/3$ there can be two (for a wide range of proper combinations of $s < 1$ and γ parameters including the range of a sufficiently small s) or no (for sufficiently large $s < 1$ and γ values) EWCSs. In the case of two EWCSs, we identify the one with smaller α_0 as the counterpart of the usual EWCS in the Newtonian limit, while the second one with larger α_0 as a novel solution describing the collapse of a highly compact general SPS with strong non-Newtonian self-gravity. For spherical gas clouds with larger $s < 1$ values, the absence of EWCSs is due to the absence of general SPSs under the predominantly strong non-Newtonian self-gravity. We note here that the existence of two or no general SPSs for $\gamma > 4/3$ is similar to the result of Oppenheimer & Volkoff (1939) on the neutron star problem, except that their physical system has a finite boundary. In their general relativistic formalism which has effectively $4/3 < \gamma \leq 5/3$, the number of equilibrium solutions runs from one (non-relativistic) to two (non-relativistic and relativistic), and then to zero as the compact stellar mass increases. It would be very interesting to extend the self-similar general relativistic analysis of Cai & Shu (2005) for a GP gas sphere and examine the number of possible EWCSs with event horizons. For massive spherical clouds with an ineffective heat transfer, the polytropic index γ can be physically larger than $4/3$. We expect such analysis will give two or no EWCSs when the formalism of general relativity is completely taken into account.

Approaching the Newtonian gravity limit of $s \rightarrow 0$, the behaviors of the sonic critical curve differ for $\gamma < 4/3$ and $\gamma > 4/3$, respectively. For the case of $\gamma < 4/3$, the sonic critical curve does not change much. For the case of $\gamma > 4/3$, the sonic critical curve (closed loop) enlarges itself, and the outer side of the loop extends to infinity gradually. Thus in the extreme Newtonian gravity limit of $s = 0$, only one EWCS remains inside a finite radius r for any values of γ .

4.2 Other continuous self-similar solutions

By specifying proper values of v_0 and α_0 and integrating inwards from a certain sufficiently large x , various continuous dynamic self-similar solutions can be constructed.

In Figure 3, the two parameters $\{\gamma, s\}$ are chosen from the Type C regime, and thus the sonic critical loop does not appear. The function for negative reduced speed $-v(x)$ versus x for a group of continuous self-similar solutions are numerically obtained and displayed in Figure 3. The dotted

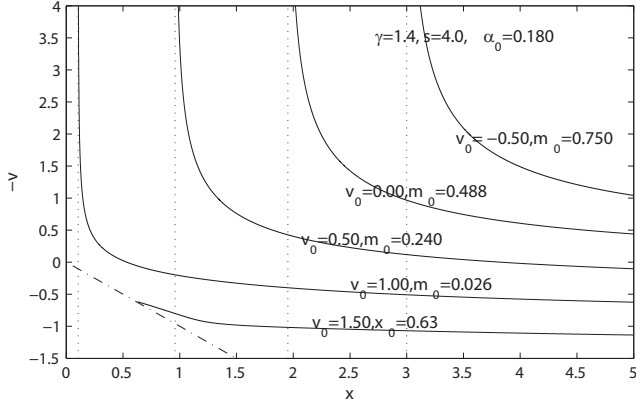


Figure 3. Numerical self-similar dynamic solutions with $\gamma = 1.4$ and $s = 4.0$ in the type C regime. Four dotted vertical lines indicate the boundaries of central black holes in each solution. The corresponding masses and radii of central black holes increase with time in a self-similar manner. Neither sonic critical curves nor EWCSs exist. The lowest solution touching the straight dash-dotted ZML $v = x$ at $x_0 = 0.63$ has a central spherical void in dynamic self-similar expansion instead of a growing central black hole. Expanding void solutions can be constructed in sequence by further increasing the value of velocity parameter v_0 . In general, numerical solutions with $v_0 > 0$ (outflow), $v_0 = 0$ (static), and $v_0 < 0$ (inflow) are all possible.

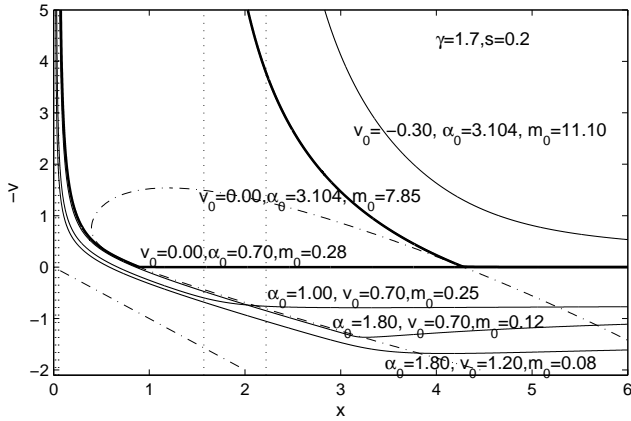


Figure 4. Numerical self-similar dynamic solutions with $\gamma = 1.7$ and $s = 0.2$ in the type B regime. The dash-dotted curve is the sonic critical curve. The straight dash-dotted line at the lower left corner is the ZML. The two heavy solid curves are the two possible EWCSs. Several self-similar solutions crossing the sonic critical line twice are also shown; they usually involve smaller α_0 values. The dotted straight vertical lines mark the expanding radii of the growing central black holes. Key pertinent parameters are marked along solution curves. It is possible to construct dynamic self-similar solutions with $v_0 > 0$, $v_0 = 0$ and $v_0 < 0$ far away.

straight vertical lines represent the expanding boundaries (event horizons) of the central Schwarzschild black holes, where the magnitude of the function $-v(x)$ diverges to infinity according to asymptotic analytic solution (29). Here, mass parameter α_0 is fixed at a given value of 0.180, while different numerical solutions correspond to different values of velocity parameter v_0 far away. The corresponding val-

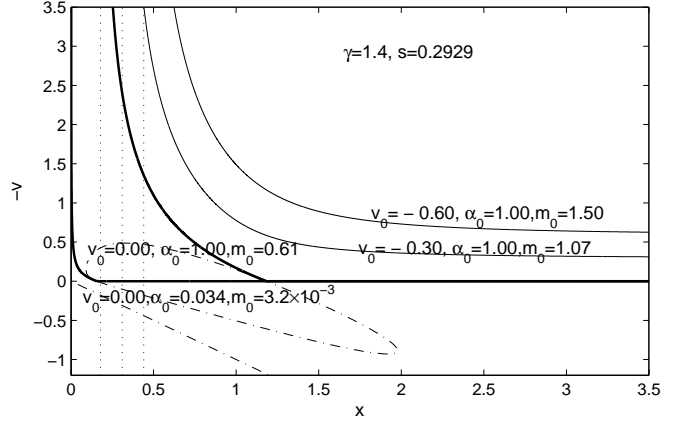


Figure 5. Numerical self-similar dynamic solutions with $\gamma = 1.4$ and $s = 0.2929$ in the type B regime. The dash-dotted loop is the sonic critical curve. The straight dash-dotted line at the lower left corner is the ZML. The two heavy solid curves are the two possible EWCSs. Two self-similar solutions (both with $v_0 < 0$) not crossing the sonic critical curve are also shown; in general, they have larger α_0 values. Dotted vertical lines on the left side indicate the expanding boundaries of central black holes. Pertinent parameters are marked along the solution curves.

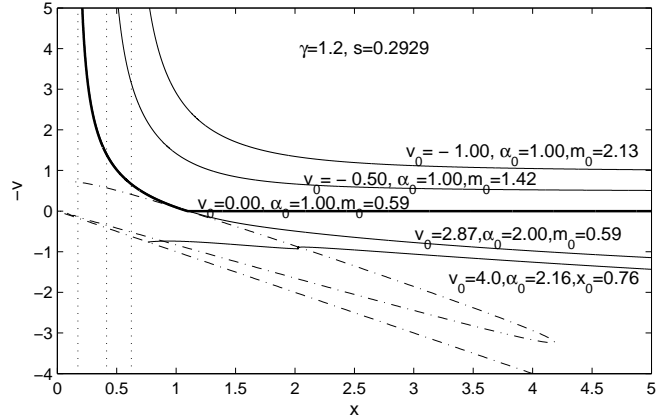


Figure 6. Numerical self-similar solutions with $\gamma = 1.2$ and $s = 0.2929$ in the type A regime. The partial dash-dotted elongated loop broken near $x = 0$ is the sonic critical curve. The straight dash-dotted line at the lower left corner is the ZML. The heavy solid curve is the only EWCS. The lowest solution coincides with the EWCS inside the expansion-wave front. The dotted straight vertical lines indicate the expanding radii of the growing central black holes. Key pertinent parameters are marked along the solution curves. It is also possible to construct a void solution that passes across the elongated sonic critical loop (broken at small x) twice smoothly.

ues of m_0 are also indicated as well. Generally speaking, a higher outflow velocity v_0 far away corresponds to a smaller size for the central black hole. When the velocity parameter v_0 becomes large enough, there is no central black hole but instead an expanding void emerges at the center, where both pressure and mass density of the gas vanish. In astrophysics, a central energy source (or a “fire ball”) is needed in order to carve out and retain such a dynamically expanding void into a massive envelope or shell. In various pertinent

contexts, we have recently explored several astrophysical applications of such dynamical voids in self-similar expansions (e.g., Lou & Wang 2012; Lou & Zhai 2009, 2010; Lou & Hu 2010). With conceptual consistency, dynamical self-similar void in expansions can also emerge with the Paczynski-Wiita gravity. The slope of $v(x)$ of the void solution when x approaches the ZML $x - v = 0$ is well determined analytically in Appendix A.

In both Figures 4 and 5, we show several constructed solutions for chosen $\{\gamma, s\}$ pairs in the Type B regime. In Figure 4, pertinent parameters are $\gamma = 1.7 > 5/3$ and $s = 0.2$, while in Figure 5, we specify the parameter pair $\gamma = 1.4 > 4/3$ and $s = 0.2929$. The two possible EWCSs with central event horizons are shown by the heavy solid curves. Generally speaking, there are two main branches of solutions. One branch of solutions does not cross the oval sonic critical curve, including the outer expansion-wave solution, as shown in Figure 5 by the light solid curves. The other branch of solutions crosses the oval sonic critical curve twice, and the inner expansion-wave solution belongs to this kind. The light solid curves in Figure 4 correspond to this branch of solutions. They usually have a larger value of mass parameter α_0 and a smaller or less massive central black hole than the former branch of solutions when their velocity parameter v_0 values are comparable to each other.

Figure 6 is plotted to demonstrate self-similar solutions of two coupled nonlinear ODEs (13) and (14) in the Type A regime. We take $\gamma = 1.2$ and $s = 0.2929$. As is easily seen, the elongated sonic critical curve breaks in the vicinity of the origin. The only EWCS with central event horizon is shown by the heavy solid curve. Several other solutions with different v_0 values are displayed in light solid curves above the EWCS. The lowest solution in this figure is connected smoothly onto the EWCS at the expansion-wave front on the sonic critical curve. These two solutions correspond to two different derivatives dv/dx across the sonic critical curve. The analysis of the two possible first derivatives dv/dx across the sonic critical curve can be found in Appendix A.

Discontinuities in the first derivative dv/dx may arise when solutions cross the sonic critical curves (e.g. Whitworth & Summers 1985). Different values of the velocity first derivative dv/dx may lead to distinct behaviors around the central collapsing core. A few explicit examples are shown in Figures 7 and 8. In Figure 7, solutions c , d and e are constructed by integrating inwards from the same yet sufficiently large x , with the same initial reduced density α_0 but slightly different initial reduced velocity v_0 . Compared to solution c in Figure 7 which has a black hole (event horizon) at the center, solutions d and e cross the sonic critical curve with a jump in dv/dx , leading to corresponding voids around the center in self-similar expansions. They nevertheless have similar dynamic behaviors at sufficiently large x . In Figure 8, solutions c , d and e are obtained by integrating outwards from small x . They have the same behavior before hitting the sonic critical curve. Solution c does not actually go across the sonic critical curve, and has a discontinuity in dv/dx when touching the sonic critical curve; this is implemented by adopting the two eigenvalues of dv/dx on the sonic critical curve. Solution d crosses the sonic critical curves twice, and has a discontinuity in dv/dx when hitting the sonic critical curve for the second time. Solution e fea-

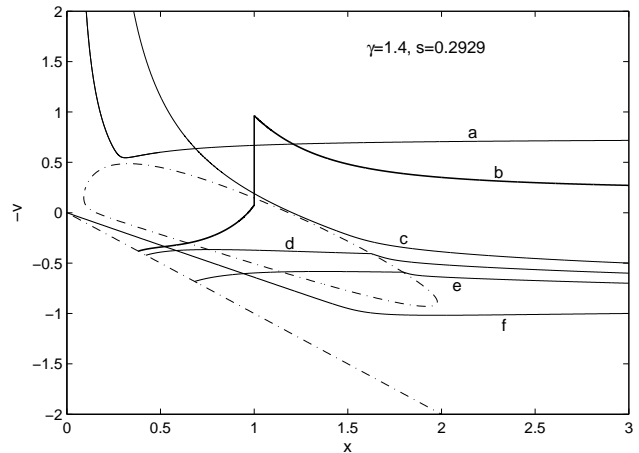


Figure 7. Shown here are several examples of self-similar dynamic solutions with $\gamma = 1.4$ and $s = 0.2929$. The closed dash-dotted curve is the sonic critical loop and the straight dash-dotted line represents the zero mass line (ZML). We obtain these numerical solutions by specifying α_0 and v_0 at a sufficiently large x and integrating towards small x . For solutions a and c , there are event horizons for black holes at the center of collapse. Solutions d and e have discontinuities in the first derivative dv/dx when crossing the sonic critical loop, and have expanding voids inside the gas cloud. Solutions c , d and e have similar behaviors at large x , but differ when encountering the sonic critical curve. Solution b involves a shock wave across the sonic critical loop and a central expanding void. Solution f smoothly reaches the center $x = 0$ very closely without singularity, and is obtained by carefully tuning the initial α and v at large x . If one tunes the initial velocity v larger (smaller) while keeping the initial α invariant, the integrated solution will develop an expanding void (black hole) at the center. Thus, f solution appears to separate solutions with central voids and solutions with central black holes. Solutions b , d , and e have central voids expanding outwards in self-similar manners.

tures a shock wave solution and a central black hole with an expanding event horizon which will be discussed further in the next subsection.

Solution f in Figure 7 and solution b in Figure 8 are examples of solutions reaching the origin at $x = 0$, with neither black holes nor voids around the center. In terms of solution structures, they appear to represent a kind of gradual transition from central voids to central Schwarzschild black holes. These solutions are obtained by carefully tuning the initial values of α_0 and v_0 for inward integration at a sufficiently large x . Starting from solution f in Figure 7 as an example, if one tunes the initial velocity v_0 to be larger (smaller) while keeping the initial α_0 unchanged, the integrated numerical solution will give rise to a void (or black hole) around the center. Solution b has a discontinuity in dv/dx when crossing the sonic critical curve, and if one tunes the initial velocity v_0 to be larger (or smaller) while keeping the initial α_0 unchanged, the integrated numerical solution leads to a void.

The reduced mass density functions $\alpha(x)$ of numerical solutions in Figure 8 are plotted in Figure 9 in correspondence. We use the same labels a , b , c , d , e as those of their corresponding reduced velocities $v(x)$ shown in Figure 8. For solutions a , c , d , e with black holes at the center, the

mass density drops to zero rapidly when approaching the Schwarzschild radius (i.e., event horizon). This is an important effect due to a rapid acceleration the gas experienced near the event horizon of a black hole. For solution *b* which continues to the origin $x = 0$, the mass density diverges at the center, as concluded in Section 3.4 for $\gamma < 4/3$. At large radii, the reduced mass density functions all drops with a $1/x^2$ scaling. When a solution hits the sonic critical curve, there is a discontinuity in $d\alpha/dx$ in association with the discontinuity in dv/dx .

4.3 Dynamic shock waves in self-similar expansion

It is possible to construct self-similar dynamic solutions with expanding shocks. Across a shock wave front, discontinuities in gas mass density, radial flow velocity, gas pressure and specific entropy occur. By setting the constant proportional coefficient $\mathcal{C} = 1$ with no loss of generality in equation (9) for the reduced form of GP EoS with $\gamma \neq 4/3$, we need to assign different sound parameters k_+ and k_- for the upstream and downstream sides of a shock front. Accordingly, we use subscript indices $+$ and $-$ to distinguish variables at upstream and downstream sides of a shock, respectively. In principle for shock conditions in the framework of reference co-moving with the shock, we require conservations of mass, radial momentum and energy across a shock. More specifically, the jump conditions for shock wave solutions can be obtained from coupled nonlinear ODEs (11), (13) and (14) immediately by integration from the left-hand side (downstream) of the discontinuous point to the right-hand side (upstream). In terms of reduced functions $\alpha(x)$ and $v(x)$, we can cast these jump conditions across the shock as

$$k_-^{1/2} x_- = k_+^{1/2} x_+, \quad (46)$$

$$k_-^{3/2} (x_- - v_-) x_-^2 \alpha_- = k_+^{3/2} (x_+ - v_+) x_+^2 \alpha_+, \quad (47)$$

$$k_- [\alpha_- (x_- - v_-)^2 + \beta_-] = k_+ [\alpha_+ (x_+ - v_+)^2 + \beta_+], \quad (48)$$

$$\begin{aligned} k_-^{3/2} \left[\frac{\alpha_-}{2} (x_- - v_-)^3 + \frac{\gamma \beta_- (x_- - v_-)}{(\gamma - 1)} \right] \\ = k_+^{3/2} \left[\frac{\alpha_+}{2} (x_+ - v_+)^3 + \frac{\gamma \beta_+ (x_+ - v_+)}{(\gamma - 1)} \right], \end{aligned} \quad (49)$$

where the upstream (+) and downstream (-) reduced dimensionless pressures $\beta_{\pm} = \alpha_{\pm}^{3\gamma-2} (x_{\pm} - v_{\pm})^{2(\gamma-1)} x_{\pm}^{4(\gamma-1)}$ are defined at the shock front. For an isothermal gas of $\gamma = 1$, we replace the term $\beta/[\alpha(\gamma - 1)]$ in the equations by its limit $\ln[\alpha^3(x - v)^2 x^4]$. The law of thermodynamics for the increase of specific entropy from the upstream side to the downstream side further requires the flow velocity relative to the shock must be supersonic on the upstream side and subsonic on the downstream side.

Examples of self-similar shock solutions are given as solution *b* in Figure 7 and as solution *e* in Figure 8. In order to avoid the ambiguity brought by using different sound parameters k_{\pm} , we multiplied the downstream v_- and x_- in the presentation of solution *b* in Figure 7 by a factor $(k_-/k_+)^{1/2}$ (the upstream side of the shock naturally involves k_+), while we multiplied the upstream v_+ and x_+ in the presentation of solution *e* in Figure 8 by a factor $(k_+/k_-)^{1/2}$ (the downstream side of the shock naturally involves k_-). The reduced

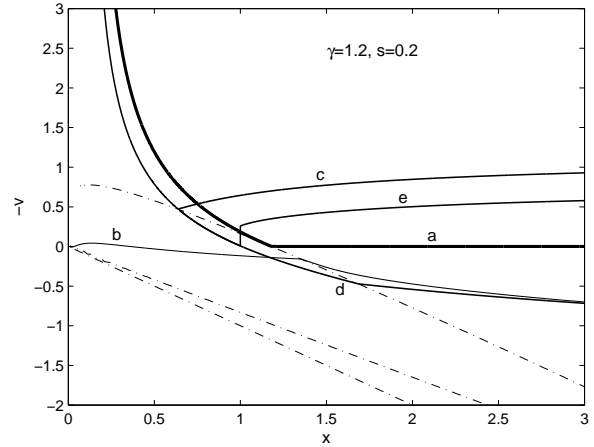


Figure 8. Numerical solutions with $\gamma = 1.2$ and $s = 0.2$. The dash-dotted curve broken in two segments is the sonic critical curve, while the straight dash-dotted line is the ZML. Solution *a* in boldface line is the EWCS with an event horizon of central black hole. Both solutions *b* and *c* have discontinuities in dv/dx when crossing the sonic critical curve. Solution *b* smoothly reaches $x = 0$, $v = 0$, and has a discontinuity in dv/dx when crossing the critical curve. It is obtained by integrating inwards with carefully chosen initial values of α_0 and v_0 at a sufficiently large x . Solutions *c*, *d* and *e* are obtained by integrating outwards from small x . Two eigenvalues for the first derivative dv/dx are allowed at the sonic critical curve. Solution *c* does not cross the critical curve smoothly and has a discontinuous dv/dx there. Solution *d* crosses the sonic critical curve twice. Solution *e* is obtained by creating a shock across the sonic critical curve. This is an example of a black hole inside an expanding shock.

mass density function $\alpha(x)$ of the shock solution *e* in Figure 8 is shown in Figure 9 in correspondence.

We note that there is a void instead of a black hole at the center of solution *b* in Figure 7, shrouded within the shock wave front. Physically, this may imply that the central shock wave inside a progenitor during a supernova explosion may delay the formation of a black hole and/or other compact remnants, supporting a transient void at the center of explosion (Lou & Wang 2012). Such a void could be filled with electron/positron e^\mp pair plasma, high-energy neutrinos, and intense radiation field. When the shock weakens and peters out, a black hole or a compact remnant may or may not form under the stellar self-gravity in a fall-back process, depending on how fast the massive envelope expands.

In principle by our formalism with the Paczynski-Wiita gravity, one could further explore many more abundant solutions with various weak discontinuities across the sonic critical curve, for instance, double-shock solutions, as has been done in some earlier works within the Newtonian gravity formalism (e.g., Whitworth & Summers 1985; Lazarus 1981). These solutions may be used to describe specific physical processes associated with mass collapses to form black holes, which will be pursued in separate papers.

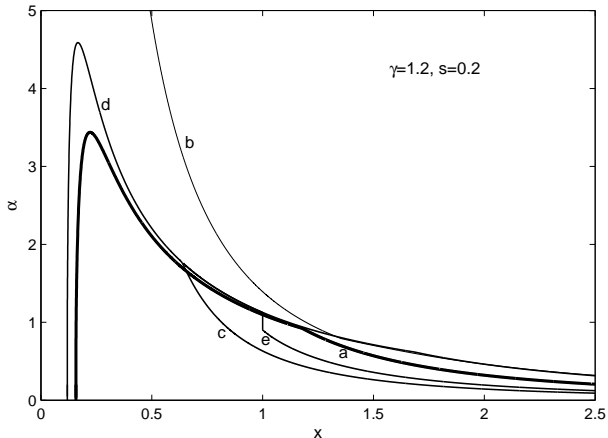


Figure 9. Reduced mass density function $\alpha(x)$ corresponding to numerical solutions for $v(x)$ in Figure 8 with the parameter pair $\gamma = 1.2$ and $s = 0.2$. The labels *a, b, c, d, e* denote the reduced mass density function of the corresponding velocity solutions denoted by the same labels in Figure 8. At the Schwarzschild radius, the reduced mass density $\alpha(x)$ drops to zero, as shown in equation (30). Discontinuities in $d\alpha/dx$ occur in accompany with the corresponding discontinuities in dv/dx when the solutions cross the sonic critical curve. For solution *b* where there is no void or black hole at the center, the mass density diverges as $x \rightarrow 0$; it represents a kind of transition between voids and event horizons of central black holes. For the shock wave solution *e*, the reduced mass density function $\alpha(x)$ is discontinuous at the shock.

5 PHYSICAL SELF-SIMILAR SOLUTIONS AND REALISTIC BLACK HOLE SYSTEMS

The possible values for the two parameters s and α_0 to adopt may take the following physical considerations into account. By referring to self-similar transformation (7), one readily derives the following expression

$$s = \frac{2(p/\rho)}{c^2 \alpha^{3\gamma-3} (x-v)^{2\gamma-2} x^{4\gamma-4}}, \quad (50)$$

where p and ρ are the gas pressure and mass density, while c is the speed of light in vacuum. As a simple way to estimate the above expression, we take the limit of $x \rightarrow \infty$ (corresponding to $t \rightarrow 0$ for a fixed r or $r \rightarrow \infty$ at a fixed t), where $\alpha \rightarrow \alpha_0/x^2$ and $v \rightarrow \text{constant}$. If we regard p/ρ approximately as the square of the sound speed denoted by u_S^2 , we have a simple estimation

$$s\alpha_0^{3\gamma-3} = 2 \frac{u_S^2}{c^2}. \quad (51)$$

Another equation that can be easily derived from self-similar transformation (7) is

$$\frac{GM}{r} = k \frac{m(x)}{x}. \quad (52)$$

We then regard GM/r as the square of the Keplerian velocity u_K^2 and thus for large x , equation (52) above yields

$$s\alpha_0 = 2 \frac{u_K^2}{c^2}, \quad (53)$$

which is usually much smaller than 1. At the event horizon or boundary of a black hole, we have $GM/r_g = c^2/2$ and

$x = sm_0$ where m_0 is the reduced dimensionless black hole mass. After a time t of sustained self-similar mass accretion and collapse, the radius r_g for the event horizon of a black hole increases linearly with time t according to equation (31) as $r_g = s^{3/2} m_0 c t / 2^{1/2}$. Naturally, another physical requirement is simply $s^{3/2} m_0 < 2^{1/2}$ such that the expansion speed of Schwarzschild radius r_g should remain less than c .

In plausible mass collapse and accretion processes for a black hole inside a galactic bulge or central region in a cluster of galaxies, the gas temperature can be as high as $\sim 10^7$ K to $\sim 10^8$ K or even higher. The Keplerian velocity u_K and the sound speed u_S are more or less in the same order of magnitudes (due to the Virial theorem) around $\sim 10^2$ km s^{-1} to $\sim 10^3$ km s^{-1} . Such dynamic mass collapse and accretion processes may be possibly represented by an EWCS with a parameter range of $s \sim 10^{-7}$ to $\sim 10^{-5}$ and $\alpha_0 \sim 1$; in the limit of $s\alpha_0 \rightarrow 0$, it is easily seen from condition (44) for an EWCS with an event horizon that $\alpha_0 \sim 1$. The physical meaning of parameter s is the square of the ratio of the sound speed u_S (or comparably, the Keplerian velocity u_K) to c in the regime of very large radius r (i.e. sufficiently far away from an accreting central supermassive black hole – SMBH). By our sample calculations, these EWCSs usually have a reduced black hole mass $m_0 \sim 0.1$ to 1. Therefore a SMBH with a mass of $\sim 10^9 M_\odot$, or equivalently with a Schwarzschild radius of $\sim 3 \times 10^9$ km, may rapidly emerge through a quasi-spherical dynamic mass collapse process in a range of timescales from $\sim 10^5$ to $\sim 10^7$ years with an important proviso for the presence of sustained mass reservoirs surrounding the central singularity of spacetime. In other words for cosmological contexts, it is conceivable to find rare hypermassive black holes (HMBHs) in an even higher mass range of $\sim 10^{10} M_\odot$ to $\sim 10^{12} M_\odot$ as long as hypermassive matter reservoirs (e.g. rich clusters of galaxies with $\sim 10^{15} M_\odot$) could be formed and maintained in the universe and they could sustain quasi-spherical dynamic mass collapses towards central SMBHs/HMBHs. Our estimated SMBH growth time is fairly short as compared to the age of typical galaxies ($\sim 10^{10}$ yrs), mainly because quasi-spherical dynamic collapses with large effective accreting areas are much more efficient than disk accretions due to the well-known difficulty of removing disk angular momentum. Such behaviors are similar to the familiar Bondi accretion (Bondi 1952; Bondi & Hoyle 1944), which nevertheless describes a steady-state spherical mass accretion of a conventional polytropic gas onto a gravitating central mass point (i.e., the gas self-gravity is ignored in the well-known Bondi model).

Quasi-spherical dynamic mass collapses might indeed dominate in the early stages of black hole formation and growth, when a seed black hole (or a singularity) remains small and surrounded by a gas cloud, or a remnant supermassive star (SMS), that is sufficiently dense and in large amount (e.g. Hoyle & Fowler 1963; Fowler 1964; Begelman 2009). Under such favorable conditions, a black hole forms and accretes from an almost spherically symmetric massive envelope or reservoir, and mass accretions are effective in all directions. It might be plausible to suspect that SMBHs in most galaxies probably might have experienced an early fast growth phase when conditions are favorable in the very early epochs of the universe well before the formation of disk structures of galaxies, and powerful quasars with high red

shifts $z > 6$ and 7 or even more (e.g. Mortlock et. al. 2011) and AGNs may appear during such unusually fast mass collapses and accumulations. Early universe and later epochs may allow cold dark matters (DMs) to form loosely bound systems or pre-galaxies under the self-gravity (e.g. Peebles 1982; Blumenthal et. al. 1984), which are most probable to take a grossly spherical structure. Such quasi-spherical DM structures may be present in the universe ubiquitously without being detected by a large fraction so far. They become more easily detected when they dynamically interact with normal matters in gas phase leading to active radiations. As an example, nearby DM dominated dwarf galaxy Segue 1 may reveal an extremely important clue along this line of reasoning (e.g. Xiang-Grüss, Lou, & Duschl 2009). Some extremely high mass density peaks may also exist in the early universe according to numerical simulations, due to density fluctuations and sound waves left after the extremely hot and dense initial cosmological stages (e.g. Tolman 1934; Ford & Parker 1977; Lukash 1980; Mukhanova et al. 1992; Lyth & Riotto 1999). Such fluctuating spacetime may allow relatively local quasi-spherical mass collapse processes of early black holes, and SMBHs with masses exceeding $\sim 10^9 M_\odot$ or $\sim 10^{10} M_\odot$ (i.e. HMBHs) are possibly formed in several million years (e.g. Hu, Shen, Lou & Zhang 2006). Over the past several decades, growing evidences show the extremely high red shift bright quasars and many AGNs are most likely powered by accreting SMBHs (e.g. Begelman et al. 1984; Rees 1984; Kormendy & Richstone 1995 and extensive references therein), while the rapid formation of extremely massive compact objects within such a short timescale in the early universe is still not well understood. Through the above physical estimates and analyses, we propose that when quasi-spherical dynamic collapses and accretions are available with enough supporting mass reservoirs, the growth rates of SMBHs may be able to reach a sensible level.

We briefly compare our theoretical model analysis with the simulations on general relativistic collapses of the supermassive stars (SMS) (Hoyle & Fowler 1963) up to a mass limit of $\sim 10^6 M_\odot$ (e.g. Shibata & Shapiro 2002; Linke et. al. 2001; Saijo & Hawke 2009; Montero et. al. 2012), which are strikingly similar to ours here. All simulations show a rapid increase of the inflow velocity when approaching the black hole event horizons, which agrees with our conclusion qualitatively. In most simulations, the velocity as a function of radius indeed shows certain invariant patterns with increasing time, but not necessarily self-similar. The absence of self-similar collapses in most simulations may be related to an initial global perturbation (a sudden reduction of global pressure), which might not be physical. We suspect that for perturbations triggered at the central region, collapses in a self-similar form may be very likely to emerge. In a realistic astrophysical system, the pressure instability usually starts from the center. We expect future simulations based on such central local perturbations to test this scenario. We note that the timescale of forming a seed SMBH in the simulations is only $10 \sim 10^2$ yrs, much shorter than that estimated here. The reason is that a SMS is a far denser and more compact object (supporting nuclear reactions) than a spherical cloud that we consider here; a SMS is much faster to collapse below the Schwarzschild radius.

Under more violent conditions of forming stellar mass black holes during supernova explosions, the central core temperature may reach $\sim 10^{11}$ K to $\sim 10^{12}$ K or even higher, and the surrounding gas envelope may become extremely relativistic. The sound speed u_S may approach the relativistic upper bound of $c/3^{1/2}$ (e.g. Weinberg 1972), and the Keplerian velocity u_K may also be comparable to c . With these estimates, the value of s parameter may lie within the range of $0.1 \sim 1$, while $\alpha_0 \sim 1$ with $\alpha = \alpha_0/x^2$ scaling in the regime of large x . If the emergence of central stellar-mass black holes under these conditions are estimated by our self-similar dynamic collapse solutions, the timescale of a complete formation would be within $\sim 10^{-3}$ s. This short dynamic timescale is one to two orders of magnitude less than that of the supernova explosion process including stellar core collapse and the emergence of a powerful rebound shock. This dynamic timescale appears reasonable and suggestive, though a realistic supernova explosion process would be much more involved to model general relativistic space-time structures (Oppenheimer & Snyder 1939; Tolman 1939; Misner & Sharp 1964, 1965; Misner 1965), very high-energy nuclear physics (Bethe 1990 and references therein) and various hydrodynamic instabilities (Blondin et al. 2003; Buras et al. 2006; Arnett & Meakin 2011; Cao & Lou 2009, 2010; Lou & Lian 2011). Shock wave collapse solutions show the possibility of forming black holes within the supernova rebound shock, outside which the outer envelopes expand rapidly. Shock wave solution shown in Figure 8 allows inward gas flows while propagating shock energy outward due to the self-similar expansion. It might be possible that rebound shocks in supernovae work in this way by some mechanism, avoiding the shock difficulties met in unsuccessful explosions of most numerical simulations (e.g. Dessart et. al. 2006; Buras et. al. 2006; Nordhaus et. al. 2010). Besides, self-similar dynamic solutions with a central expanding void inside the gas sphere may indicate other possibilities for the fate of a powerful supernova from a massive progenitor; if due to some unknown processes certain configurations are formed, supernova explosions may leave a much rarefied central region, expelling most stellar envelope materials outwards (e.g., possibly for SN1987A).

Asymptotic solutions (29) and (30) for $v(x)$ and $\alpha(x)$ show that gas materials being swallowed are greatly accelerated and diluted when approaching the Schwarzschild black hole, and all particles would behave as high-energy free particles. For polytropic index $\gamma > 1$, it is further seen from two relations (50) and (8) that the sound speed $u_S = (p/\rho)^{1/2}$ near the black hole event horizon tends to vanish. Drastic infall acceleration of atoms and charged particles would give rise to powerful X -ray and γ -ray emissions, leading black hole systems to become as astrophysical X -ray and γ -ray sources (for stellar mass black holes), quasars or AGNs (for SMBHs residing in elliptical galaxies and galactic bulges or even HMBHs in clusters of galaxies). With extremely diluted environments, a thermal dynamic equilibrium can hardly be achieved, and the produced X -rays and γ -rays may escape from a certain inner zone outside the event horizon with relatively weak absorptions. It is known from astrophysical observations for decades that X -ray sources and AGNs show hard radiation spectra which are power laws peaked at short wavelengths of X -rays and γ -rays (e.g. Barr et al. 1980; Osterbrock & Miller 1975; Koski 1978; Costero &

Osterbrock 1977). For producing such emissions with hard spectra, the mass accretion clouds need to be optically thin (e.g. Rees et al. 1982; Shapiro et al. 1976).

6 CONCLUSIONS AND SUMMARY

Gravitational core collapse of a GP gas sphere (with EoS p/ρ^γ being constant along streamlines) towards central Schwarzschild black holes is investigated in the self-similar dynamic formalism. In order to catch key features of the general relativity for black holes, we invoke the Paczynski-Wiita gravity (Paczynski & Wiita 1980) instead of the Newtonian gravity in our calculations. A new dimensionless parameter s emerges in the self-similar formalism, which corresponds to the square of the ratio of the sound speed to the speed of light, and the self-similar solutions diverge at the finite Schwarzschild radius which expands linearly in time with a finite mass accretion rate. Approaching the event horizon of the central black hole, the mass collapse velocity goes to infinity, while the gas mass density and pressure vanish.

Various semi-analytical solutions can be constructed through numerical shooting integrations by imposing proper asymptotic analytic conditions, among which the most interesting ones are the EWCSs (Shu 1977; Lou & Shen 2004; Cai & Shu 2005; Wang & Lou 2008) representing the gravitational collapse of static singular GP gas spheres. In particular, these EWCSs are shown to be closely related to the properties of the sonic critical curves. Cai & Shu (2005) worked out the EWCS for an isothermal gas of $\gamma = 1$ in the general relativistic formalism. To approximate the general relativity by the Paczynski-Wiita gravity, our GP hydrodynamic model analysis shows that for $\gamma < 4/3$, only one EWCS exists, while for $\gamma > 4/3$, there are either two (for small $s < 1$) or no (for large enough $s < 1$) such EWCSs (see Fig. 1 for more details). We would expect this conclusion to remain valid within the exact formalism of general relativity. These EWCSs may offer a sensible description for possible gravitational core collapse and accretion of nearly static GP gas spheres by the central black hole. One may also construct various self-similar dynamic solutions with non-vanishing radial flow velocities at infinity, some of which cross the sonic critical curve with or without discontinuity in the first derivatives of velocity, while others involve outgoing shocks. For self-similar solutions with high outflow velocities, the center of gas sphere may form an expanding void instead of a black hole, where both the gas pressure and the mass density vanish.

Quasi-spherical dynamic collapse may play an important role of rapidly forming SMBHs in galactic nuclei. A SMBH of mass $\sim 10^9 M_\odot$ may be formed within a timescale range of $\sim 10^5 - 10^7$ years via quasi-spherical dynamic mass **collapse**, provided there maintains an enough amount of gas materials or stars as the surrounding mass reservoirs to sustain such a process. Accordingly, SMBHs in the mass range of $\sim 10^6 - 10^9 M_\odot$ would be expected to form in a range of shorter timescales as compared to the above estimated timescale range. Of course, such SMBH formation process can be cut short if the surrounding mass reservoir cannot be sustained for some natural reasons. Moreover in the cosmological context of large-scale structure formation, it is also conceivable to form hypermassive black holes (HMBHs) in

the mass range of $\sim 10^{10} M_\odot$ to $\sim 10^{12} M_\odot$ on rare occasions of hypermassive material reservoirs (e.g. central regions of rich clusters of galaxies) as associated with large-scale mass structures in the universe. Likewise, black holes with mass less than $\sim 10^6 M_\odot$ may also exist if the quasi-spherical dynamic mass **collapse** process is interrupted under various situations. Observationally, SMBHs seem to lurk in most galactic bulges (e.g. Begelman et al. 1984; Rees 1984; Kormendy & Richstone 1995), and observations of high red shift (high- z) quasars (e.g. Mortlock et al. 2011) and AGNs further indicate an early formation of SMBHs in about one billion years since the Big Bang. Non-uniformly distributed matters and dark matters may result in pre-galaxies, proto-galaxies and high density peaks, which may possibly sustain massive reservoirs for quasi-spherical dynamic collapses towards seed black holes. Matters directly falling into the black hole experience drastic acceleration and would likely produce luminous hard X -ray and γ -ray emissions, forming quasars, AGNs or stellar ultra-luminous X -ray sources.

Estimation of the black hole formation during supernova explosions can also be made by self-similar dynamic solutions. Collapse of a massive stellar core is believed to lead to black holes (Chandrasekhar 1935; Oppenheimer & Volkoff 1939; Oppenheimer & Snyder 1939). Under extremely relativistic conditions inside a massive progenitor during supernova with the sound speed less than yet comparable to the speed of light, the timescale of forming stellar mass black holes is estimated to be $\sim 10^{-3} s$, which is ~ 1 to 2 orders of magnitudes shorter than that of the supernova explosion. Self-similar shock solutions also show that the rebound shock energy is possible to propagate outward against the inflow of gas materials. We suggest that such shocks may appear in the explosion of a massive supernova and leave black holes behind in the collapsed core. By extensive explorations, we note a further physical possibility that a supernova explosion blows all the stellar core matter away, creating a highly rarefied central void in expansion, as implied by self-similar solutions with a central void. In this case there might be no compact objects left, as has been suspected for the absence of central activities in SN1987A (e.g. Lou & Wang 2012).

ACKNOWLEDGEMENTS

This research was supported in part by the Ministry of Science and Technology (MOST) under the State Key Development Program for Basic Research grant 2012CB821800, by the NSFC grants 10373009, 10533020, 11073014 and J0630317 at Tsinghua University, by the Tsinghua University Initiative Scientific Research Program, by Tsinghua Centre for Astrophysics, and by the Yangtze Endowment, the SRFDP 20050003088, 200800030071 and 20110002110008, and the Special Endowment for Tsinghua College Talent (Tsinghua XueTang) Program from the Ministry of Education (MoE) at Tsinghua University.

REFERENCES

Abramowicz M. A., Beloborodov, A. M., Chen, X.-M., Iguemshchev, I. V., 1996, *A&A*, 63, 221

- Abramowicz M. A., 2009, *A&A*, 500, 213
 Arnett W. D., Meakin C., 2011, *ApJ*, 733, 78
 Bahcall J. N., Ostriker J. P., eds, 1997, *Unsolved Problems in Astrophysics*. Princeton Univ. Press, Princeton
 Barr P., et. al., 1980, *MNRAS*, 193, 549
 Begelman M. C., 2009, *MNRAS*, 402, 673
 Begelman M. C., Blandford R. D., Rees M. J., 1984, *Rev. Mod. Phys.*, 56, 255
 Bethe H. A., 1990, *Rev. Mod. Phys.*, 62, 801
 Blondin J. M., Mezzacappa A., DeMarino C., 2003, *ApJ*, 584, 971
 Blumenthal G., Faber S. M., Primack J., Rees M. J., 1984, *Nature*, 311, 517
 Bondi H., 1952, *MNRAS*, 112, 195
 Bondi H., Hoyle F., 1944, *MNRAS*, 104, 273
 Buras R., Janka H. Th., Rampp M., Kifonidis K., 2006, *A&A*, 457, 281
 Cai M. J., Shu F. H., 2003, *ApJ*, 583, 391
 Cai M. J., Shu F. H., 2005, *ApJ*, 618, 438
 Cao Y., Lou Y.-Q., 2009, *MNRAS*, 400, 2032
 Cao Y., Lou Y.-Q., 2010, *MNRAS*, 403, 491
 Chandrasekhar S., 1935, *MNRAS*, 95, 207C
 Chandrasekhar S., 1939, *An Introduction to the Study of Stellar Structure*, Dover Publications, Inc., London
 Churazov E., Sunyaev R., Forman W., Böhringer H., 2002, *MNRAS*, 332, 729
 Costero R., Osterbrock D. E., 1977, *ApJ*, 211, 675
 Dessart L., Burrows A., Livne E., Ott C.D., 2006, *ApJ*, 645, 534
 Fabian A. C., Canizares C. R., 1988, *Nature*, 333, 829
 Ferrarese L., Ford H., 2005, *Space Sci. Rev.*, 116, 523
 Ford L. H., Parker L., 1977, *Phys. Rev. D*, 16, 1601
 Fowler W. A., 1964, *ApJ*, 144, 180
 Goldreich P., Weber S. V., 1980, *ApJ*, 238, 991
 Graham A. W., Driver S. P., 2007, *ApJ*, 655, 77
 Guth A. H., 1981, *Phys. Rev. D*, 23, 347
 Haardt F., Maraschi L., 1991, *ApJ*, 380, L51
 Haardt F., Maraschi L., 1993, *ApJ*, 413, 507
 Hoyle F., Fowler W. A., 1963, *MNRAS*, 125, 169
 Hu J., Shen Y., Lou Y.-Q., Zhang S.N., *MNRAS*, 2006, 365, 345
 Kluźniak W., Lee W. H., 2002, *MNRAS*, 335, L29
 Kormendy J., Richstone D. 1995, *ARA&A*, 33, 581
 Koski A. T., 1978, *ApJ*, 223, 56
 Lazarus R. B., 1981, *SIAM J Numer. Anal*, 18, 316
 Linke F., Font J. A., Janka H.-T., Muller E., Papadopoulos P., 2001, *A&A*, 376, 568
 Lou Y.-Q., Cao Y., 2008, *MNRAS*, 384, 611
 Lou Y.-Q., Hu R.-Y., 2010, *New Astronomy*, 15, 198
 Lou Y.-Q., Jiang Y. F., 2008, *MNRAS*, 391, L44
 Lou Y.-Q., Lian B., 2012, *MNRAS*, 420, 214
 Lou Y.-Q., Shen Y., 2004, *MNRAS*, 348, 717
 Lou Y.-Q., Wang L.L., 2012, *MNRAS*, 420, 1897
 Lou Y.-Q., Wang W.G., 2006, *MNRAS*, 372, 885
 Lou Y.-Q., Wu Y.H., 2012, *MNRAS*, 422, L28
 Lou Y.-Q., Zhai X., 2009, *ApSS*, 323, 17
 Lou Y.-Q., Zhai X., 2010, *MNRAS*, 408, 436
 Lukash V. N., 1980, *JETP Lett.*, 31, 11
 Lynden-Bell D., 1969, *Nature*, 223, 690
 Lynden-Bell D., Pringle J. E., 1974, *MNRAS*, 168, 603
 Lyth D. H., Riotto A., 1999, *Phys. Rep.*, 314, 1
 Magorrian J. et al., 1998, *AJ*, 115, 2285
 Marconi A., Hunt L. K., 2003, *ApJ*, 589, L21
 Matteo T. D., Fabian A. C., Rees M. J., Carilli C. L., Ivison R. J., 1999, *MNRAS*, 305, 492
 Matteo T. D., Allen S. W., Fabian A. C., Wilson A. S., Young A. J., 2003, *ApJ*, 582, 133
 McConnell N. J., Ma C.-P., Gebhardt K., Wright S. A., Murphy J. D., Lauer T. R., Graham J. R., Richstone D. O., 2011, *Nature*, 480, 215
 Misner C. W., 1965, *Phys. Rev.*, 137, B1360
 Misner C. W., Sharp D. H., 1964, *Phys. Rev.*, 136, B571
 Misner C. W., Sharp D. H., 1965, *Phys. Letters*, 15, 279
 Mocanu G., Grumiller D., 2012, *Phys. Rev. D*, 85, 105022
 Montero P. J., Janka H. T., Muller E., 2012, *ApJ*, 749, 37
 Mortlock D. J. et. al., 2011, *ArXiv e-prints*, 1106.6088
 Mukhanova V. F., Feldman H. A., Brandenberger R. H., 1992, *Phys. Rep.*, 215, 203
 Nordhaus J., Brandt T. D., Burrows A., Livne E., Ott C. D., 2010, *Phys. Rev. D*, 82, 103016
 Novikov, I. D., Thorne K. S., 1973, in DeWitt C., DeWitt D., eds, *Blackholes*, Gordon and Breach Press, Paris, 343
 Nowak M. A., Wagoner R. V., 1991, *ApJ*, 378, 656
 Oppenheimer J. R., Volkoff G. M., 1939, *Phys. Rev.*, 55, 374
 Oppenheimer J. R., Snyder H., 1939, *Phys. Rev.*, 56, 455
 Osterbrock D. E., Miller J. S., 1975, *ApJ*, 197, 535
 Paczynski B., Wiita P. J., 1980, *A&A*, 88, 23
 Peebles P. J. E., 1982, *ApJ*, 263, L1
 Rees M. J., 1984, *ARA&A*, 22, 471
 Rees M. J., Begelman M. C., Blandford R. D., Phinney E. S., 1982, *Nature*, 295, 17
 Ricotti M., 2007, *ApJ*, 662, 53
 Rybicki G. B., Lightman A. P., 1979, *Radiative Processes in Astrophysics*, Wiley-Interscience Press, New York
 Saijo M., Hawke I., 2009, *Phys. Rev. D*, 80, 064001
 Semerák O., Karas V., 1999, *A&A*, 343, 325
 Shakura N. I., Sunyaev R. A., 1973, *A&A*, 24, 337
 Shapiro S. L., Lightman A. P., Eardley D. M., 1976, *ApJ*, 204, 187
 Shen Y., et. al., 2009, *ApJ*, 697, 1656
 Shen Y., et. al., 2011, *ApJS*, 194, 45
 Shibata M., Shapiro S. L., 2002, *ApJ*, 572, L39
 Shu F. H., 1977, *ApJ*, 214, 488
 Stuchlík Z., & Kovár J., 2008, *Int. J. Mod. Phys. D.*, 17, 2089
 Sunyaev R. A., & Titarchuk L. G., 1980, *A&A*, 86, 127
 Tolman R. C., 1934, *Proc. Nat. Acad. Sci. USA*, 20, 3
 Tolman R. C., 1939, *Phys. Rev.*, 55, 364
 Wandel A., 1999, *ApJ*, 519, L39
 Wandel A., 2002, *ApJ*, 565, 762
 Wang W. G., Lou Y. Q., 2008, *ApSS*, 315, 135
 Whitworth A., Summers D., 1985, *MNRAS*, 214, 1
 Xiang-Gruess M., Lou Y.-Q., Duschl W. J., 2009, *MNRAS*, 400, L52

APPENDIX A: PROPERTIES OF $V(X)$ NEAR THE SONIC CRITICAL CURVE AND THE ZERO MASS LINE

First, we consider the sonic critical curve with $x - v \neq 0$ (i.e., the elliptical-shape loop; while the ZML $x - v = 0$

and the possible expanding void solutions will be considered separately). The sonic critical curve is determined by simultaneously setting both sides of two nonlinear ODEs (14) and (11) to zero. Therefore, from the LHS of nonlinear ODE (14), we have on the sonic critical curve

$$\gamma \frac{\beta}{\alpha} = (x-v)^2. \quad (\text{A1})$$

Note that $\beta/\alpha = \alpha^{3\gamma-3}(x-v)^{2\gamma-2}x^{4\gamma-4}$; therefore specifically for $1 < \gamma < 2$, we have $\alpha \rightarrow 0$ when approaching the sonic critical curve. From nonlinear ODE (11), we have

$$\frac{2}{x} + \frac{1}{\alpha} \frac{d\alpha}{dx} = \frac{1}{(x-v)} \frac{dv}{dx}. \quad (\text{A2})$$

Utilizing the L'Hôpital rule and two relations (A1) and (A2) above, a quadratic equation for the first derivative of velocity dv/dx in the vicinity of the sonic critical curve is obtained from the vanishing two sides of nonlinear ODE (14), viz.

$$\begin{aligned} (\gamma+1) \left(\frac{dv}{dx} \right)^2 + \left[(4\gamma-6) - (4\gamma-4) \frac{(x-v)}{x} \right] \frac{dv}{dx} \\ + (4\gamma-2) \left(\frac{x-v}{x} \right)^2 - \frac{(2\gamma-2)(4\gamma-2)}{\gamma} \frac{(x-v)}{x} \\ + \frac{(2\gamma-2)(2\gamma-3)}{\gamma} + \frac{m}{(x-sm)^3} \left(\frac{x+sm}{x-v} - 2 \right) = 0, \end{aligned} \quad (\text{A3})$$

where the reduced enclosed mass $m(x)$ is given explicitly by algebraic relation (8). The two roots of dv/dx from equation (A3) can be properly chosen for distinct solutions passing across the sonic critical curve smoothly.

We now focus on the ZML $x-v=0$. As we always expect a positive enclosed mass $m(x)$, the difference $x-v$ should therefore be non-negative for a possible physical solution. Assuming that the first derivative of $v(x)$ near the ZML $x-v=0$ approaches a constant value h , that is

$$\frac{dv}{dx} = h, \quad (\text{A4})$$

which immediately leads to an approximate expansion

$$x-v = (1-h)(x-x_0), \quad (\text{A5})$$

where x_0 is the coordinate for our self-similar solution to touch the ZML $x-v=0$. Then by solving nonlinear ODE (A2), we arrive at the asymptotic solution for $\alpha(x)$ near the ZML in the power-law form of

$$\alpha = \alpha_1 (x-x_0)^{h/(1-h)}, \quad (\text{A6})$$

where α_1 is an integration constant. Physically, we would require that $m = (x-v)x^2\alpha$ remains finite at $x=x_0$ (it should vanish on the ZML, as no solution is physically allowed to cross the ZML); thus we simply impose the inequality $h < 1$. Substitution of the above asymptotic solution into nonlinear ODE (14) determines the h value. There are two roots of h parameter. The first root h_1 is

$$h_1 = \frac{2(1-\gamma)}{\gamma} \leq 0, \quad (\text{A7})$$

with the coefficient $\alpha_1 > 0$ being an arbitrary constant. The second root h_2 is given by

$$h_2 = \frac{2(2-\gamma)}{(\gamma+1)} \geq 0, \quad (\text{A8})$$

where the constant coefficient α_1 satisfies the condition

$$h_2 [1-h_2]^{4-2\gamma} = [\gamma h_2 + 2\gamma - 2] \alpha_1^{3\gamma-3} x_0^{4\gamma-4}. \quad (\text{A9})$$

APPENDIX B: DERIVATION OF EQUATION FOR THE SONIC CRITICAL CURVE

The sonic critical curve of two coupled nonlinear ODEs (13) and (14) can be readily derived by setting the both sides of these two nonlinear ODEs to vanish, namely

$$(x-v)^2 - \gamma \frac{\beta}{\alpha} = 0, \quad (\text{B1})$$

$$\frac{(x-v)x^2\alpha}{[x-s(x-v)x^2\alpha]^2} + \frac{(2\gamma-2)}{(x-v)} \frac{\beta}{\alpha} - \frac{2(x-v)^2}{x} = 0, \quad (\text{B2})$$

$$\frac{(x-v)x^2\alpha}{[x-s(x-v)x^2\alpha]^2} + \left[\frac{(2\gamma-2)}{(x-v)} - \frac{2\gamma}{x} \right] \frac{\beta}{\alpha} = 0, \quad (\text{B3})$$

where the reduced gas pressure $\beta = \alpha^{3\gamma-2}(x-v)^{2\gamma-2}x^{4\gamma-4}$ is defined by GP EoS (10) according to the specific entropy conservation along streamlines. In reference to equation (B1), only one of the two algebraic equations (B2) and (B3) is independent; this would guarantee the consistency of our model analysis. Eliminating the reduced mass density α by proper substitutions, we reach the following algebraic equation for the sonic critical curve

$$\frac{x-v}{x} - \frac{\gamma-1}{\gamma} = \frac{\gamma^{\frac{1}{3-3\gamma}}(x-v)^{\frac{\gamma+1}{3\gamma-3}-1}x^{2/3}}{2[x-s\gamma^{\frac{1}{3-3\gamma}}(x-v)^{\frac{\gamma+1}{3\gamma-3}}x^{2/3}]^2} \quad (\text{B4})$$

as stated in the main text.

APPENDIX C: NUMBER OF ROOTS IN THREE DISTINCT REGIMES OF FIGURE 1

By defining a function $f(\alpha_0) \equiv 2\alpha_0^{3\gamma-4}(1-s\alpha_0)^2$ in reference to equation (44), our task is to actually solve equation $f(\alpha_0) = 1$ for possible roots of α_0 . For astrophysical applications, we should demand inequality $1-s\alpha_0 > 0$, and thus physical roots of α_0 fall within the open interval $(0, 1/s)$.

It is easily seen for $\gamma < 4/3$, both $\alpha_0^{3\gamma-4}$ and $(1-s\alpha_0)^2$ decrease monotonically as α_0 increases; therefore, $f(\alpha_0)$ keeps decreasing from infinity to zero within the open interval $(0, 1/s)$ and only one α_0 root exists.

For $\gamma > 4/3$, $\alpha_0^{3\gamma-4}$ increases as α_0 increases. The first derivative of $f(\alpha_0)$ with respect to α_0 is simply

$$\frac{df}{d\alpha_0}(\alpha_0) = 2\alpha_0^{3\gamma-4}(1-s\alpha_0)^2 \left[\frac{(3\gamma-4)}{\alpha_0} - \frac{2s}{(1-s\alpha_0)} \right], \quad (\text{C1})$$

indicating that $f(\alpha_0)$ first increases and then decreases with increasing α_0 , taking zero values at both $\alpha_0 = 0$ and $\alpha_0 = 1/s$. Function $f(\alpha_0)$ then reaches its maximum value f_{\max} at $\alpha_{0M} = (3\gamma-4)/[(3\gamma-2)s]$ with f_{\max} given by

$$f_{\max} = \frac{8[(3\gamma-4)/s]^{3\gamma-4}}{(3\gamma-2)^{3\gamma-2}}. \quad (\text{C2})$$

For $f_{\max} > 1$, there exist two roots for α_0 . For $f_{\max} < 1$, there will be no roots for α_0 . For $f_{\max} = 1$, the two roots of α_0 become degenerate. The pertinent numerical results are displayed in Figure 1. Specifically for $s < 1-1/\sqrt{2} = 0.2929$, the maximum value f_{\max} is always greater than 1, which

ensures the existence of two roots for α_0 . For other pairs of γ and s in the type B regime of Figure 1, there are also two roots for α_0 . One needs to check whether the two α_0 roots are less than $1/s$ to be physically useful.

This paper has been typeset from a $\text{\TeX}/\text{\LaTeX}$ file prepared by the author.